Characterization and Absolute QE Measurements of Delta-Doped N-Channel and P-Channel CCDs

Blake C. Jacquot*[a], Steve P. Monacos, Todd J. Jones, Jordana Blacksberg, Michael E. Hoenk, Shouleh Nikzad

[a]Jet Propulsion Laboratory, California Institute of Technology, 4800 Oak Grove Drive, Pasadena, CA, USA 91109

ABSTRACT

In this paper we present the methodology for making absolute quantum efficiency (QE) measurements from the vacuum ultraviolet (VUV) through the near infrared (NIR) on delta-doped silicon CCDs. Delta-doped detectors provide an excellent platform to validate measurements through the VUV due to their enhanced UV response. The requirements for measuring QE through the VUV are more strenuous than measurements in the near UV and necessitate, among other things, the use of a vacuum monochromator, and good camera vacuum to prevent chip condensation, and more stringent handling requirements. The system used for these measurements was originally designed for deep UV characterization of CCDs for the WF/PC instrument on Hubble and later for Cassini CCDs.

Keywords: Delta doping, CCD, QE

*bjacquot@jpl.nasa.gov; phone 1 818 354-0515; fax 1 818 393-4663; jpl.nasa.gov

1. INTRODUCTION

A sensitive measurement such as QE requires careful attention to a variety of factors including source selection, filter selection, reference detector calibration and selection, and system calibration among other factors. Further complicating the difficulty is the need to accurately determine system gain in order to correctly interpret signals recorded from a CCD. The most common method, photon transfer, requires care because noise sources must be treated properly and the gain is found by fitting a curve on a log-log plot. A small change in the fit conditions can result in a relatively large change in the perceived system gain.

Compounding the difficulty are the added requirements of testing through the VUV. For wavelengths in this range a vacuum system is needed to avoid atmospheric absorption and to avoid water or other condensations on the imager. Further, very stringent cleanliness requirements are introduced due to the need to avoid burning hydrocarbons on surfaces that reduce system throughput and result in error. In this paper we treat the most pressing considerations when testing from the VUV through the NIR.

2. ENVIRONMENT CONSIDERATIONS FOR THE VACUUM ULTRAVIOLET

Measurements from 100nm to 200nm need a vacuum monochromator for good integrity due to atmospheric absorption [1]. Alternative approaches may use a nitrogen purged environment. At JPL, an Acton 1m vacuum monochromator with either 300g/mm or 600g/mm grating is used to characterize devices from Lyman-α (121.6nm) through the near infrared (Fig. 1). This system was originally designed for deep UV characterization of CCDs for the WF/PC instrument on Hubble and later for Cassini CCDs.

High Energy, Optical, and Infrared Detectors for Astronomy IV, edited by Andrew D. Holland, David A. Dorn
Proc. of SPIE Vol. 7742, 77420I · © 2010 SPIE · CCC code: 0277-786X/10/$18 · doi: 10.1117/12.857694

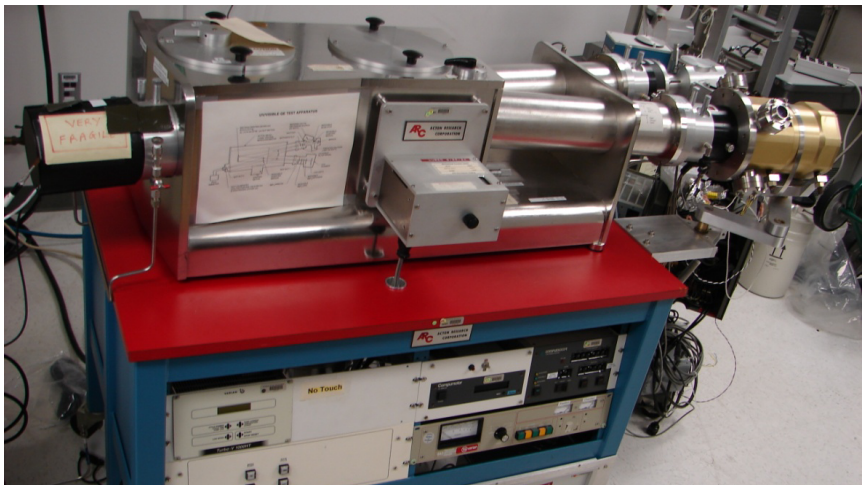

Fig. 1. 1-meter Acton vacuum monochromator used in measurements. This system was originally used for deep UV characterization of CCDs for the WF/PC instrument on Hubble and later for Cassini CCDs.

Beyond a vacuum environment, VUV measurements have great sensitivity to surface contamination [2]. Hydrocarbons can deposit on components of the system (e.g. grating, mirrors, windows, diffusers, diodes, etc.) and become permanently burned in place with VUV radiation. If not properly guarded against, the system state can shift and render calibration meaningless. Periodic calibration becomes necessary to monitor for this effect.

3. ELIMINATION OF SYSTEMATICS

The first line of defense against measurement error is the elimination of systematics that can affect the measurement.

3.1 Sources

Proper choice of light sources aids the elimination of out-of-band leak. Red leak, the most commonly-discussed type, results from any wavelength longer than the desired range contaminating the signal. Causes of red leak include poorly filtered light from a source with much stronger emission at wavelengths longer than the measurement wavelength. Blue leak is equally troubling if unmanaged. Contamination from wavelengths shorter than the desired wavelength (e.g. from strong UV sources) or second order light from a monochromator can render absolute measurement meaningless.

To guard against out-of-band leak, we have chosen to use a deuterium source for illumination from Lyman-alpha to approximately 350nm and a tungsten-halogen source from 360nm to the near infrared. The deuterium source has the advantage of strong emission between 100-200nm and a lesser, relatively flat emission profile above this. Tungsten-Halogen exhibits a blackbody radiation profile with a peak around 800-1000 nm.

In regions where the sources are strong (e.g. below 200nm for Deuterium and 500-900 nm for Tungsten-Halogen) guarding against out-of-band leak becomes simpler due to the strong signal relative to out-of-band wavelengths. However in regions where neither source has strong emission (e.g. 250nm-400nm) one must exercise special care to ensure light leak does not occur or at least is not an appreciable fraction of the total signal.

3.2 Filtering

Beyond source selection, the choice of filters is the other major consideration in the elimination of systematic error. As mentioned above, out-of-band leak can destroy a high-quality measurement. Some origins of out-of-band leak include stray light reflections of walls of the monochromator, stray light reflection off the monochromator grating, and second-order light contamination from the grating. Properly chosen bandpass and longpass filters can dramatically reduce most of these sources of error.

The first concern when choosing a filter is consideration of second-order light from the monochromator. Longpass filters for use with monochromators (commonly called “order sorting” filters) provide excellent protection from this phenomenon. Monochromator gratings allow both the first order light containing the wavelength of interest and the

second order containing half the wavelength of interest to reach the detector [3]. For instance a desired wavelength of 500nm will also contain a smaller amount of 250nm light. Filters should be chosen to eliminate the second order light.

Broadband reflection off gratings or other items in the signal chain will also result in signal contamination and requires filtering. Directly observing the grating when tuned for 500nm will show a bright green light with specks of white light contamination. The best approach involves using bandpass filters at the source to restrict the range of light allowed into the monochromator. The more narrow the bandpass filter, the greater the purity of light at the desired wavelength. However, practical concerns of the available physical space for filters may necessitate acceptable tradeoffs between filter choice and optimization.

Our measurement setup allows for a 7-position filter wheel which we populated with 6 filters and an open position (Table 1). For the deuterium source we use no filter, Fused Silica, or Pyrex (obtained from Princeton Instruments). The deuterium spectrum below 164nm is relatively strong, relieving concerns about red leak. Fused Silica and Pyrex are longpass filters that guard primarily against blue leak from the deuterium source. Note that Fused Silica with its approximately 160nm cutoff can be used up to twice this wavelength before second order light starts to contaminate the signal, so we discontinue its use around 300nm. The same reasoning applies to Pyrex, though twice its cutoff of approximately 300nm is well beyond the usable range of the deuterium source. In the difficult to measure region of 250nm-400nm (where neither source is strong) we deploy bandpass filters. The relatively narrowband U-340 filter with 85nm passband provides excellent filtering against red leak from the Tungsten-Halogen source. The B-390 filter has a l*a*rger passband at 125nm and also provides filtering against red leak. The longpass GG-420 filter provides order sorting filtering for the Tungsten-Halogen source up to approximately 840nm (double the cutoff). However the grating used in this measurement does not extend beyond 650nm. The U-340, B-390, and GG-420 filters were obtained from Edmund Optics.

Table 1. Filters used in QE characterization

Filter	Utilized Range (nm)	Note	Source
None	116-164	Must limit exposure due to high energy of radiation	Deuterium
Fused Silica	164-300	Long-pass filter with cutoff at ~160nm	Deuterium
Pyrex	300-350	Long-pass filter with cutoff at ~300nm	Deuterium
U-340	360-370	Hoya bandpass filter, 85nm passband	Tungsten-Halogen
B-390	380-450	Hoya bandpass filter, 125nm passband	Tungsten-Halogen
GG-420	500-650	Schott longpass filter with cutoff at ~420nm and full transmission starting at ~495nm	Tungsten-Halogen

Efforts to measure the amount of out-of-band leak indicate the above filtering scheme is successful. The Tungsten-Halogen source allows for convenient characterization since a separate filter can be placed in front of the source to limit light reaching the filter wheel. For example, when tuned to 340nm with the U-340 filter selected in the filter wheel and a separate GG-420 2" square longpass filter sitting in front of the source, the total current read by the a picoammeter was 0.1pA as compared to 4.8pA when the GG-420 filter was removed. This indicates light leak above the 420nm cutoff of the longpass filter contributes approximately 2% to the total signal. Similar tests for the B-390 filter (also using the GG-420 filter) when tuned to 390nm indicate an out-of-band leak accounts for <1.4% of total signal. Tuning to 450nm and using the GG-420 filter in the 7-position filter wheel with a separate longpass filter with 630nm cutoff indicates out-of-band leak accounts for <10% of total signal, an unacceptable amount. The signal to noise ratio improves dramatically when moving to longer wavelengths due to increasing strength of the source and is the primary reason why 500nm was selected as the transition point between the B-390 and GG-420 filter. Out-of-band leak tests for the Deuterium source

comparing readings from using a Fused Silica and Pyrex filter at 121.6nm, 200nm, and 250nm propitiously indicate out-of-band leak contributes less than 0.5% of total signal.

3.3 Reference Detectors

The choice of reference detectors can help eliminate measurement error. Often CsTe photodiodes are used since they are blind to visible light. However, we have chosen broadband silicon photodiodes as our calibrated standards due to the large wavelength range and the desire to not change diodes during measurement, thus reducing opportunities for hydrocarbon contamination and human error. During initial system calibration two photodiodes are used in place of the CCD imager to measure light levels as seen by the CCD. A NIST-calibrated IRD AXUV-100G is used to measure light between 116-254nm. A second IRD-calibrated UVG-100 photodiode is used to measure between 250-1100nm. A separate uncalibrated IRD AXUV-100G sits permanently at another port within the monochromator and provides a reference reading for system calibration (discussed below). In principle the IRD AXUV-100G can cover the entire wavelength range desired, but calibration lead time constraints necessitated the 2-diode approach.

As with other components, the photodiode response is very sensitive to hydrocarbon contamination. Further, the passivating oxides can get damaged by high-energy UV radiation [4-5]. NIST typically randomly screens photodiodes from lot run to determine expected damage from UV exposure and will only release devices that meet their specifications.

3.4 Optics and Signal Chain Components

Careful selection of optics and components is needed for compatibility with VUV illumination. MgF_2 is the most common material for transmissive windows and coatings and is used extensively in our system. Reflective surfaces typically use Al coated with MgF_2 as a protective coating. Many of the materials will degrade with prolonged exposure to UV light, necessitating periodic recalibration. UV light exposure should be minimized when possible to avoid this damage.

3.5 Cleaning and Bakeout of Components

Any component entering the vacuum system should experience a substantial cleaning and bakeout procedure (aside from very sensitive components such as mirrors, gratings, and windows). Typically, we sonicate metals for 30 minutes with an ultrasonic cleaning solution followed by 5 minutes of acetone and 5 minutes of IPA sonication and finally a vacuum bakeout. Typical vacuum bakeout conditions are 120ºC (or higher) for 16-48 hours. Any organic entering the system (e.g. O-rings, printed circuit boards, electronic cables) should experience a similar cleaning procedure with the exception of the acetone bath. Bakeout of organics is extremely critical for minimizing outgassing in the vacuum system, which can irrevocably foul surfaces with hydrocarbons.

3.6 Flat Field

In many of our measurements we want to compare various antireflective (AR) coatings and bare surfaces on the same device, demanding a flat field so that all surfaces see equal illumination. We realize a flat field by using 2 MgF_2 Diffusers of 1” diameter which sit at the end of the monochromator signal chain and approximately 6” in front of the detector. This configuration allows for less than 5% light intensity variation across an approximately 2cm x 2cm surface, as measured directly by a CCD. A third diffuser could be used, but the light flux is so low that potential error introduced by lengthy exposure times outweighs the marginal improvement in flat field.

Often an integrating sphere is used to create a flat field, but this is difficult for VUV measurements due to material constraints and need for a vacuum environment. Variations of polytetrafluoroethylene (PTFE, e.g. Teflon) are commonly used for coating the inside of spheres and providing a reflective surface. While PTFE works well for visible light, it absorbs in the VUV. Adding further complication, most integrating spheres are not vacuum compatible. Though we had discussions with a company about making a vacuum-compatible integrating sphere with Al coating, the costs were prohibitive and we were able to obtain excellent flat fields with the above methods.

3.7 Baffles

Reflection from sidewalls can cause error in measurement and so baffles should be deployed to collimate the light wherever possible. This becomes more crucial after the diffusers and before the detector due to the spherical emanation

of light which can easily reach and reflect from sidewalls. We use a series of 3 baffles spaced 1" apart prior to the CCD to collimate the light.

3.8 System Calibration

The first step in system calibration is determining the tuning of the monochromator grating wavelength against programmed mechanical counter reading. To accomplish this, several known wavelengths must be determined and fit using a polynomial function. In our system we used Lyman-alpha (121.6nm) and several narrowband interference filters (340nm, 500nm, 640nm) for a total of 4 data points. We then used a 3rd order polynomial to fit the data and interpreted the tuning of the monochromator with the results.

We rely on a global method of calibrating the measured light rather than a component-by-component method. Our procedure consists of tuning to a given wavelength and measuring the reading from a calibrated photodiode sitting in place of the target CCD and comparing this reading to another photodiode at a separate port selected by a diverter mirror. This near real-time measurement provides a ratio of the light at the two ports which can then be used to interpret readings from the CCD. For instance, if at 200nm we see a reading of 10pA from CCD port diode and 175pA at the diverter mirror selected port, the ratio (10pA/175pA) can be used to determine the light reaching the CCD when we have a fresh reading from the diverter mirror selected port during the QE measurement. Typically we see sources exhibit less than 10% variation in light level from measurement to measurement.

Another common method of system calibration is to measure the transmission and reflectance of each element along the signal chain and compile them for a global throughput. However, this method does not work if the final measurement requires a flat field. The flat field (either created by an integrating sphere or diffusers) is most easily and accurately measured directly.

As mentioned above, the system will drift over time, thus requiring periodic recalibration. If the calibration shifts materially, effort should be made to determine the primary source of the change.

4. CRYOGENIC OPERATION AND VACUUM CONSIDERATION

4.1 Temperature and Vapor Pressure of Ice

Cryogenic measurements of CCDs require attention to the vacuum condition in order to avoid buildup of condensation or ice on the detector surface that degrades measurements. High-quality scientific measurements of CCDs require cooling the detector to cryogenic temperature in order to minimize dark current. However as temperature drops, so does the vapor pressure of ice [6-7]. For instance at -50ºC the vapor pressure of ice is approximately $3x10^{-2}$ Torr. If the camera base pressure is above this level, ice will deposit on the detector surface. At -80ºC the vapor pressure of ice is $4.1x10^{-4}$ Torr. Our camera base pressure operates at approximately $5x10^{-6}$ Torr. We typically run the detectors at -80ºC to avoid ice buildup. We have demonstrated hysteresis in measurements when operating at -130ºC with ice as the likely culprit. Data in Figure 2 shows this effect. Absolute QE is presented later in this paper.

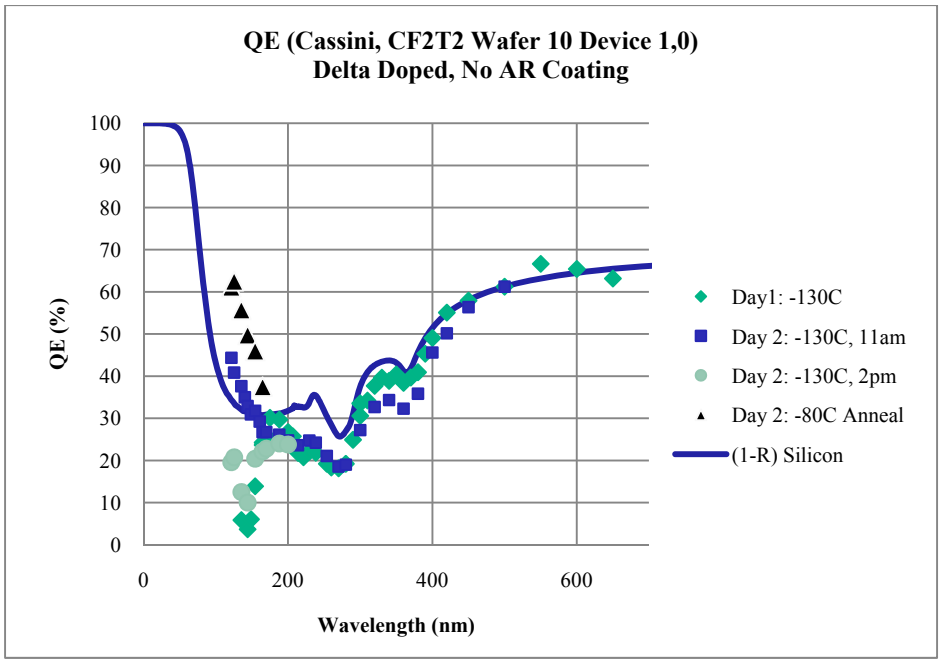

Fig. 2. Demonstration of measurement hysteresis when operating at -130ºC with ice as the likely culprit. Measurements made after holding temperature at -130ºC for extended period of time are depressed relative to initial measurements at that temperature or after -80ºC anneal. Base pressure of camera relative to operating temperature must be considered to avoid this effect. Absolute QE measurement is presented later in this paper.

4.2 Cryogenic Design

Our liquid nitrogen-based cryogenic design keeps the detector stable to ±0.2ºC (Fig. 3). A copper cold finger assembly bolts to a roughly 1L liquid nitrogen tank within the interior of the dewar. A copper assembly connects the tank to the CCD. A proportional-integrative-derivative (PID) controller takes readings from a thermocouple located near the device and uses the information to drive a heater cartridge located in the copper assembly to stabilize the CCD temperature. Alternative approaches to this design may use a closed-cycle cooler (e.g. CRYOTIGER)

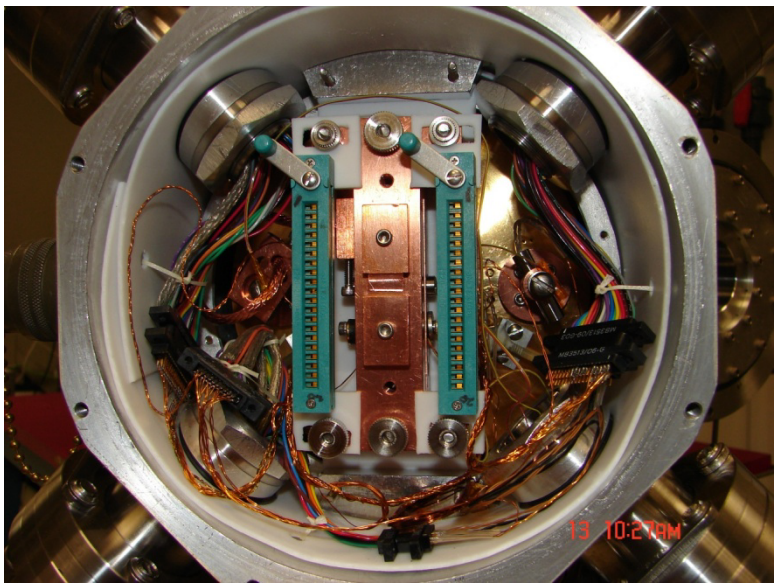

Fig. 3. Front view of CCD camera head. A liquid nitrogen tank provides cooling for the detector through a copper mount. CCD temperature is monitored with thermocouple and fed to a PID controller which adjusts a heater cartridge to maintain ±0.2ºC stability.

5. PHOTON TRANSFER MEASUREMENTS

A photon transfer curve provides the system gain used to interpret readings from the CCD and can result in substantial error if performed poorly. The measurement rests on fitting a shot-noise limited curve and finding the x-intercept where the noise is unity in Digital Number (DN) [8]. At this point, the x-intercept (or signal) is equal to the system gain. A small change in the fit conditions can result in a relatively large change in perceived system gain. Noise sources must be treated properly when extracting the shot-noise limited curve.

5.1 Obtaining Shot Noise-Limited Curve

Various methods exist for obtaining a shot-noise limited curve. The most common method involves taking two exposures under the same conditions (e.g. integration time or exposure time) starting at a zero-second exposure and working up to the point where the device starts to saturate. Differencing the two exposures for a region of interest (ROI) removes fixed pattern noise (FPN) while doubling the read and shot noise. Correcting for this doubling and then backing out the read noise obtained from either a zero second exposure or from an overscan region gives the shot noise for a given exposure time. Pairing this shot noise value with the mean of the ROI gives a shot-noise limited point for the photon transfer curve. Note, the ROI should have substantial size (e.g. 100x100 pixels) to give statistically meaningful results.

A sample photon transfer curve shows the raw data, data corrected for FPN, data corrected for FPN and read noise, and shot-noise limited curve fit (Fig. 4). At either very low or very high signal levels the shot-noise limited curve begins to deviate from the trend line due to very low signal to noise ratio or the onset of full well conditions. The slope of the shot-noise limited curve should equal 0.5. Tracing this line back to the x-axis gives the system gain in terms of electrons per digital number (e-/DN).

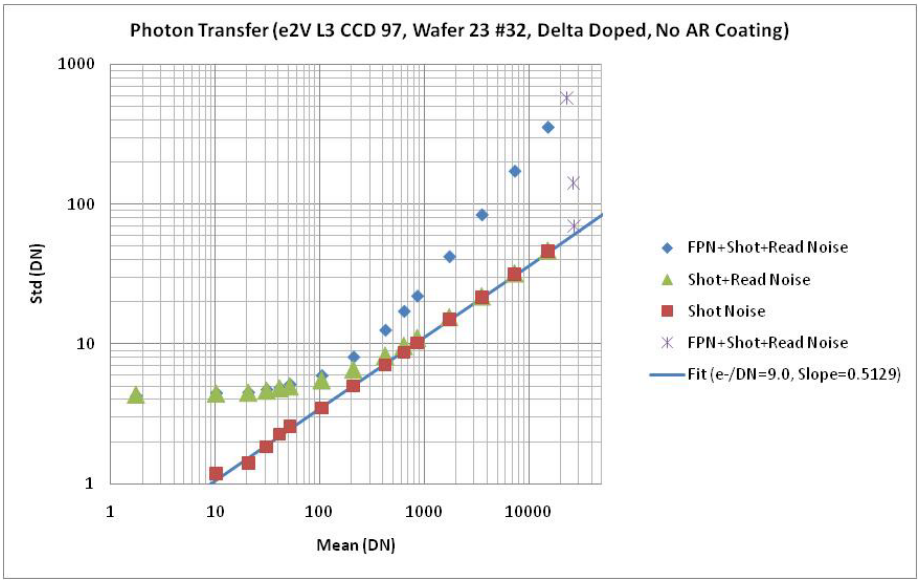

Fig. 4. Sample photon transfer curve shows the raw data, data corrected for FPN, data corrected for FPN and read noise, and shot-noise limited curve fit. For either very low or very high signal levels the shot-noise limited curve begins to deviate from the trend line due to very low signal to noise ratio or the onset of full well conditions. The slope of the shot-noise limited curve should equal 0.5. Tracing this line back to the x-axis gives the system gain in terms of electrons per digital number (e-/DN).

6. QUANTUM YIELD AND ELECTRON GAIN

Photons with energy greater than approximately 3.65eV (340nm) can generate more than a single electron-hole pair, resulting in a quantum yield greater than unity [9]. Readings from the CCD must be adjusted for this in the relevant

range in order to generate a valid quantum efficiency plot. An extrapolation of measurements made above 10eV give the following approximation:

$$\eta_i = \frac{12390}{E_{e-h}\lambda}$$

Here, η_i is the quantum yield gain (e-/photon), $E_{e\text{-}h}$ is the energy required to generate an electron-hole pair (approximately 3.65eV at room temperature for silicon), and λ is the photon wavelength in Å.

An alternative and more accurate way to obtain quantum yield is to measure it directly [10]. In this method the shot-noise limited std(DN)=1 intercept is found for a wavelength above 340nm (e.g. 400nm) and ratioed with the intercept for a wavelength where quantum yield is greater than unity. We have made initial measurements of quantum yield using this method (Fig. 5). A full photon transfer curve must be constructed for each wavelength to accurately measure the quantum yield, dramatically increasing the amount of data for an experiment and also risking UV damage of the detector.

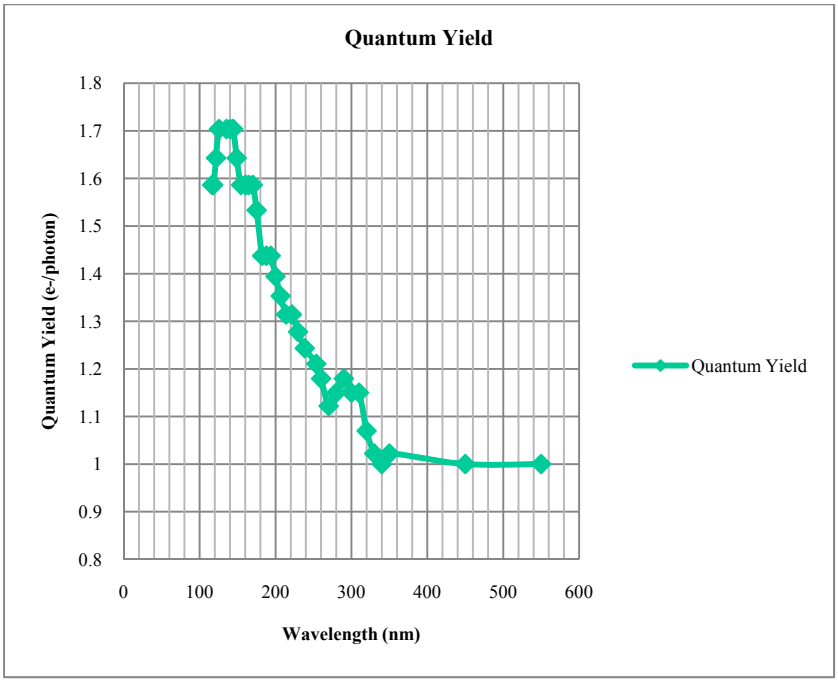

Fig. 5. Initial measurement of quantum yield resulting from creating a photon transfer curve at each wavelength of interest. The gain factor from visible wavelength is divided by the gain factor for UV wavelength to determine calculate quantum yield.

7. READOUT ELECTRONICS AND DATA PROCESSING

Electronic interface with the CCD is provided by an Astronomical Research Camera Inc. controller which captures frame information from the detector [11]. A controller box is populated with fiber optic timing board, clock driver board, utility board, and video boards and communicates through fiber optic cable with a PCI card residing in a personal computer. We collect FITs files and import them into Matlab for data manipulation and processing to gather information for photon transfer and QE curves.

8. DELTA DOPING

8.1 Delta Doping

Due to their enhanced UV response and stability of their response over a wide range (EUV-NIR) delta-doped detectors provide an excellent platform for testing and validating QE data through the VUV. Delta-doped CCDs, developed at JPL's Microdevices Laboratory have achieved stable 100% internal quantum efficiency (QE) in the visible, near UV,

and vacuum UV (VUV) regions of the spectrum [12-14]. In this approach, an epitaxial silicon layer is grown on a fully-fabricated CCD or CMOS imager using molecular beam epitaxy (MBE). During the growth, approximately a monolayer of dopant atoms is deposited on the surface, followed by a silicon cap layer for surface passivation. The dopant is incorporated within a single atomic layer at the back surface of the device, resulting in the effective elimination of the backside potential well. The measured quantum efficiency is in good agreement with the theoretical limit imposed by reflection from the Si surface.

8.2 N-Channel CCDs

Cassini CCDs were used for the study of n-channel CCDs. These 1Kx1K devices were thinned to approximately 20µm and delta doped. Characterization was conducted from the VUV to the visible wavelengths.

8.3 P-Channel CCDs

Lawrence Berkeley National Laboratory (LBNL) has developed a large-format p-channel CCD with high QE extended to 1000nm (Fig. 6) [15-16]. The devices achieve high QE in the NIR by fully depleting a 200-300µm thick lightly doped substrate of approximately 3.6-4.3 x 10^{11} cm^{-3}. The choice of p-channel instead of the conventional n-channel stemmed from findings that it was easier to produce low dark current devices and from increased radiation tolerance over n-type devices.

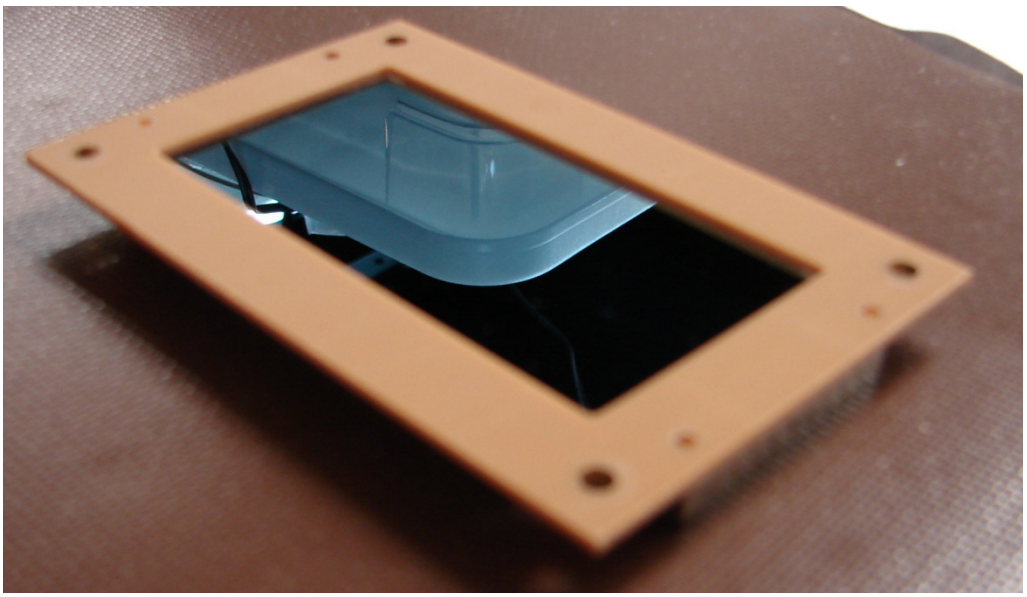

Fig. 6. Packaged, delta-doped LBNL P-Channel device

9. DEVICE PREPARATION

9.1 Backside Illumination

Front-illuminated devices present challenges for high quantum efficiency. Because of absorption of photons in the metals and gate oxides on the frontside, CCDs have limited QE in the front illumination configuration. In CMOS imagers where electronics circuitry occupy some of the pixel, the percentage of light-sensitive region to total pixel area (fill-factor) of front-illuminated devices is limited by the area required for metal traces that block photons from reaching the photosensitive region of the pixel. Backside illuminated devices can dramatically improve sensitivity. Back-illuminated imagers require thinning (substrate removal) or high resistivity substrates and full depletion.

9.2 Thinning

Fully-processed CCD die or rafts of many contiguous die, complete with aluminum contacts, are thinned by either wet or dry etching (Fig. 7). In wet etching, some 90% of the bulk silicon is removed by KOH etching. The remaining bulk silicon is etched with 1:3:8 HNA (hydrofluoric acid, nitric acid, acetic acid) which stops at the epitaxial layer of the device. Dry etching can be used in place of the KOH to remove the 90% of bulk silicon. The dry ecth process is deep reactive ion reactive ion etching (DRIE).

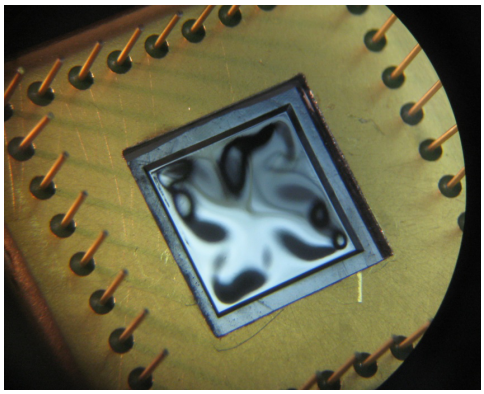

Fig. 7. Thinned and delta-doped Cassini n-channel CCD.

9.3 AR Coatings

When used, AR coatings are first modeled with TFCALC and then deposited by atomic layer deposition (ALD), thermal evaporation, or sputtering.

10. RESULTS

Data was collected at JPL for a variety of devices with n-channel and p-channel designs. The QE of p-channel devices were also measured at LBNL. After generating a photon transfer curve, flat fields were collected at a variety of wavelengths from vacuum UV through 650nm. For calculation of QE, a consistent 2D ROI was picked from the image and differenced from a similarly-timed dark integration. The mean of the net signal in coordination with other factors such as the ratio of light between photodiodes, pixel size, photodiode reading, exposure time, photodiode size, and quantum yield are used to create a quantum efficiency plot versus wavelength (Fig. 8). Here, empirical results for quantum yield were used.

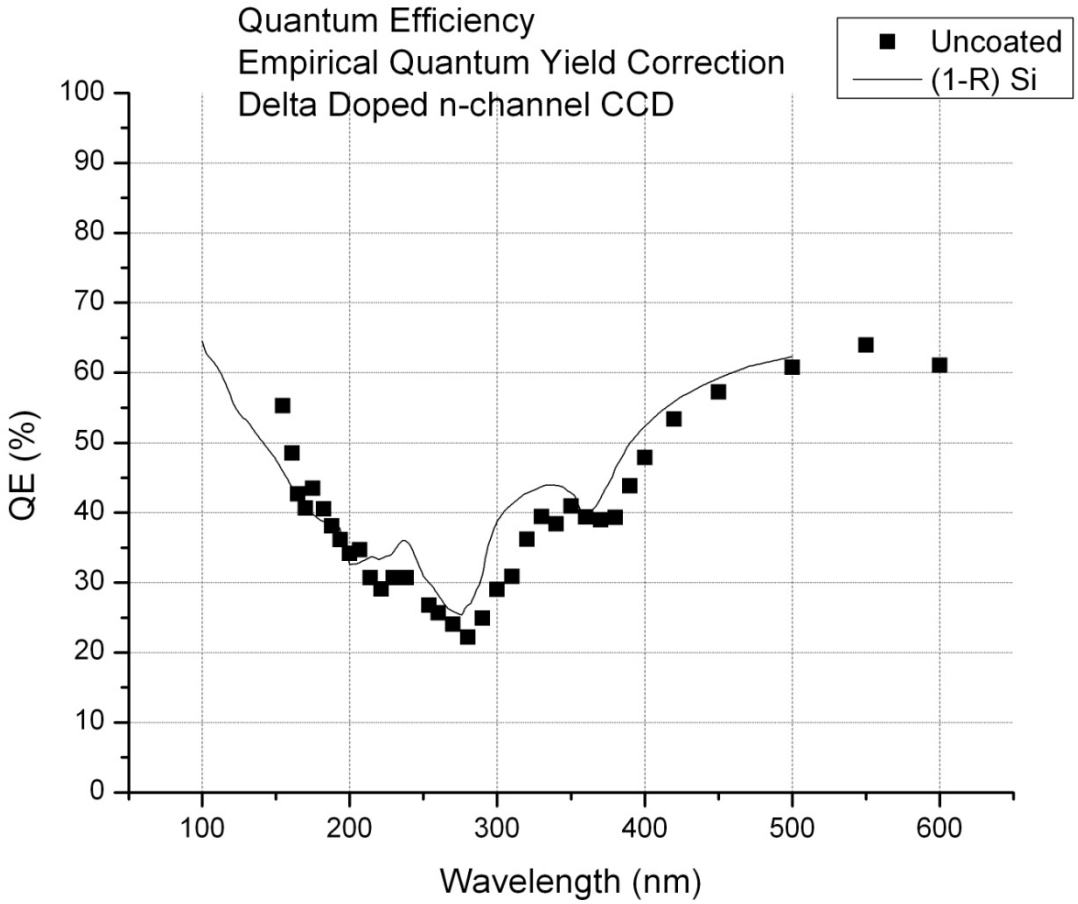

Fig. 8. Quantum efficiency measurements of thinned and delta-doped Cassini imager modeled results.

Functional p-channel devices have been analyzed at JPL but not yet for a quantitative QE measurement in the system described here. In the future quantum efficiency data will be collected for p-channel devices in this lab. A separate grating is used to obtain high-quality measurements from far UV through the near infrared. Our system is not currently calibrated for this measurement due to the current focus on VUV measurements.

11. SUMMARY

In this paper we have reviewed system requirements for QE measurements, have described JPL VUV QE characterization setup, and presented results of QE testing of delta-doped silicon CCDs at JPL. Accurate measurement of QE requires attention to the many subtleties of testing setup including source selection, filter selection, cleaning and bakeout procedures, among other issues. Critical to accurate QE measurement below 340nm is a direct measurement of quantum yield. QE measurements at JPL show good agreement with reflection-limited curves and high-quality from Lyman-alpha through 650nm.

12. ACKNOWLEDGEMENTS

We gratefully acknowledge the Patrick Morrissey for discussions on quantum yield and Tom Elliott for support of Cassini devices. We thank our collaborators at LBNL for their contributions. The research was carried out at the Jet Propulsion Laboratory, California Institute of Technology, under a contract with the National Aeronautics and Space Administration.

REFERENCES

[1] Samson, J.A., Ederer, D.L., [Vacuum Ultraviolet Spectroscopy], Academic Press, (2000).

[2] Hopkins, J., Wheale, S.H., Badyal, J.P.S., "Synergistic Oxidation at the Plasma/Polymer Interface", *The Journal of Physical Chemistry,* 33(100), 14062-14066 (1996).

[3] Proctor, J.E., Barnes, P.Y., "NIST High Accuracy Reference Reflectometer-Spectrophotometer", *Journal of Research of the National Institute of Standards and Technology*, 101(5), 619-627 (1996).

[4] Gullikson, E.M., Korde, R., Canfield, L.R., Vest, R.E., "Stable silicon photodiodes for absolute intensity measurements in the VUV and soft X-ray regions", *Journal of Electron Spectroscopy and Related Phenomena*, 80, 313-316 (1996).

[5] Lauer, J.L., Shohet, J.L., Hansen, R.W., "Measuring vacuum ultraviolet radiation-induced damage", *J. Vac. Sci. Technol. A*, 21(4), 1253-1259 (2003).

[6] Wagner, W., Saul, A., and Pruss, A., "International equations for the pressure along the melting and along the sublimation curve of ordinary water substance", *J. Phys. Chem. Ref. Data,* 23(3), 515-527 (1994).

[7] Wexler, A., "Vapor pressure formulation for water in the range 0 to 100ºC", *J. Res. Natl. Bur. Stand.*, 81A(1), 5-20 (1977).

[8] Janesick, J, [Scientific Charge-Coupled Devices], SPIE, Bellingham, Washington, (2001).

[9] Janesick, J, [Photon Transfer], SPIE, Bellingham, Washington, 17-18 (2007).

[10] Morrissey, P.F., McCandliss, S. R., Feldman, P.D., "Vacuum-ultraviolet quantum efficiency of a thinned, backside-illuminated charge-coupled device", *Applied Optics*, 32(22), 4640-4650 (1995).

[11] Leach, R.W., "Design of a CCD controller optimized for mosaics", *Publications of the Astronomical Society of the Pacific,* 100, 1287-1295 (1988).

[12] Hoenk, M.E. *et. al.*, "Growth of a delta-doped silicon layer by molecular beam epitaxy on a charge-coupled device for reflection-limited ultraviolet quantum efficiency", *Applied Physics Letters*, 61(9), 1084-1086 (1992).

[13] Nikzad, S., *et. al.*, "Delta-doped CCDs: High QE with long-term stability at UV and visible wavelengths", *Proc. SPIE 2198*, 907-915 (1994).

[14] Nikzad, S, Jones, T.J. Cunningham, T.J., Deelman, P.W., and Elliott, S.T., "Ultrastable and Uniform EUV and UV Detector", *Proc. SPIE 4139*, 250-258 (2000).

[15] Holland, S.E., Kolbe, W.F., Bebek, C.J., "Device Design for a 12.3-Megapixel, Fully Depleted, Back-Illuminated, High-Voltage Compatible Charge-Coupled Device", *IEEE Transactions on Electron Devices*, 55(3), 1725-1735 (2009).

[16] Blacksberg, J., Hoenk, M.E., Elliott, S.T., Holland, S.E., Nikzad, S., "Enhanced quantum efficiency of high-purity silicon imaging detectors by ultralow temperature surface modification using Sb doping", *Applied Physics Letters*, 87(25), 254101 (2005).